Journal of Alloys and Compounds 509 (2011) 5488–5492

Contents lists available at ScienceDirect

Journal of Alloys and Compounds

journal homepage: www.elsevier.com/locate/jallcom

Microwave-assisted synthesis of graphene–ZnO nanocomposite for electrochemical supercapacitors

Ting Lu[a], Likun Pan[a,*], Haibo Li[a], Guang Zhu[a], Tian Lv[a], Xinjuan Liu[a], Zhuo Sun[a], Ting Chen[b], Daniel H.C. Chua[b]

[a] Engineering Research Center for Nanophotonics & Advanced Instrument, Ministry of Education, Department of Physics, East China Normal University, Shanghai, China
[b] Department of Materials Science and Engineering, National University of Singapore, Singapore 117574, Singapore

ARTICLE INFO

Article history:
Received 19 November 2010
Received in revised form 22 February 2011
Accepted 23 February 2011
Available online 3 March 2011

Keywords:
Graphene
ZnO
Supercapacitors
Nanocomposite
Microwave-assisted synthesis

ABSTRACT

Graphene–ZnO nanocomposite was successfully synthesized via microwave-assisted reduction of zinc ions in aqueous solution with graphite oxide dispersion using a microwave synthesis system. The electrochemical performance of the nanocomposite was analyzed through cyclic voltammetry and chronopotentiometry tests. The results showed that as compared with pure graphene, graphene–ZnO composite exhibited an improved electrochemical capacitance of 146 F/g with good reversible charge/discharge behavior.

1. Introduction

Graphene has attracted a great deal of attention in recent years due to its excellent electronic, capacitive and mechanical properties, superior chemical stability and high specific surface area [1–9]. Graphene can be synthesized via reduction of exfoliated graphite oxide (GO) such as chemical reduction using hydrazine or $NaBH_4$, etc. [10–12], UV assisted photocatalytic reduction [13] and high temperature annealing reduction [14,15]. However, in most of the reported methods, hazardous reducing agents, high temperature or long processing time are required. Therefore, the development of facile and practical reducing methods still remains a challenging issue.

As an inexpensive, quick, versatile technique, microwave can heat the reactant to a high temperature in a short time by transferring energy selectively to microwave absorbing polar solvents with a simultaneous increase in self-generated pressure inside the sealed reaction vessel [16–24], and it has been successfully applied in the reduction of GO. Chen et al. [25] reported a rapid and mild thermal reduction of GO to graphene with assistance of microwave in a mixed solution of N,N-dimethylacetamide and water. Li et al. [26] reported an ultrafast dry microwave synthesis of graphene in very short duration (<5 s) without using reducing agents. Janowska et al. [27] synthesized large few-layer graphene sheets in aqueous of anmmonia under microwave irradiation. Murugan et al. [19] presented a facile microwave-assisted solvothermal reduction of exfoliated GO with nontoxic solvents to obtain graphene and graphene-polyaniline nanocomposite within a short reaction time of several minutes and at relatively low temperature (180–300 °C) and investigated their application as electrode materials for lithium-ion batteries and supercapacitors.

Currently one obvious challenge is to utilize these 2D carbon nanostructures as conductive carbon mats to anchor metal oxide materials to form new nanocomposite hybrid materials with potential application in optoelectronics and energy conversion devices [28–32]. In the meantime, such an attachment of metal oxide particles onto the graphene may also prevent the restack and agglomeration of graphene sheets during the reduction process due to van der Waals interactions between them [13,32]. Several investigations have been carried out to produce graphene–metal oxide nanocomposite. Kim et al. [28] reported the vertical growth of ZnO nanostructures on graphene layers using catalyst-free metal–organic vapor-phase expitaxy and investigated their photoluminescence characteristics. Zhang et al. [29] synthesized graphene–TiO_2 nanocomposite with a sol–gel method using tetrabutyl titanate and GO as the starting materials. Yao et al. [30] fabricated the graphene–SnO_2 composite electrode materials by $NaBH_4$ reduction of graphene oxide in $SnCl_2$ solution and studied their application in lithium-ion batteries. Lambert et al. [33] studied the synthesis of TiO_2–graphene nanocomposite by

* Corresponding author. Tel.: +86 21 62234132; fax: +86 21 62234321.
E-mail address: lkpan@phy.ecnu.edu.cn (L. Pan).

0925-8388/$ – see front matter © 2011 Elsevier B.V. All rights reserved.
doi:10.1016/j.jallcom.2011.02.136

hydrolysis of TiF_4 in the presence of an aqueous dispersion of GO. Williams et al. [13] and Kim et al. [34] fabricated TiO_2–graphene or ZnO–graphene nanocomposite by UV-assisted photocatalytic reduction of graphene oxide in TiO_2 or ZnO suspensions. Wu et al. [35] employed solvothermal method to prepare sandwich-like graphene–ZnO nanocomposite in ethylene glycol medium using graphene oxide as a precursor of graphene and zinc acetylacetonate as a single-source precursor of zinc oxide. Li et al. [36] reduced GO with $SnCl_2$ to gain graphene–SnO_2 composite which achieved a better capacitive behavior with a specific capacitance of 34.6 F/g in 1 M H_2SO_4 solution. In our previous work [37], graphene–ZnO and graphene–SnO_2 composite films were fabricated by ultrasonic spray pyrolysis (USP) and graphene–ZnO composite electrode exhibited higher capacitance value (61.7 F/g) as compared with graphene–SnO_2 and pure graphene electrodes. However, as promising hybrid electrode materials for electrochemical supercapacitors (ESCs), the exploration on graphene–metal oxide composite materials is not nearly enough so far. Especially the synthesis of graphene–metal oxide composite materials by microwave-assisted reaction for electrochemical supercapacitors has seldom been reported in the literature.

In this work, one-step synthesis of graphene–ZnO nanocomposite was carried out through microwave-assisted reduction of zinc ions in aqueous solution with GO dispersion using a microwave synthesis system. The electrochemical tests showed that graphene–ZnO composite exhibited an improved electrochemical capacitance of 146 F/g with good reversible charge/discharge behavior.

2. Experimental

Commercial graphite powder was used as the starting reagent for the synthesis of GO via modified Hummers method [38,39]. 10 mg $ZnSO_4 \cdot 7H_2O$ (Sinopharm chemical Reagent Co. Ltd.) was added into a 5 ml 10 mg/ml GO solution as the source of Zn element, and then the solution was sonicated for 30 min to produce uniform dispersion. A dilute NaOH solution was dropped in the solution to form a brownish-black suspension with a pH value of 9. The mixture was then put into an automated focused microwave synthesis system (Explorer-48, CEM Co.) and treated for 0.5 h at 150 °C. It was obviously found that the color of suspension had changed into purely black, indicating the successful chemical reduction of GO [40]. The as-synthesized product was isolated by filtration, washed for three times with distilled water, and finally dried in a vacuum oven at 70 °C for 24 h. Subquently, the graphene–ZnO composite was coated on graphite sheets by screen-printing method. The detailed information can be found in our previous work [37]. The specific surface area of the screen-printed graphene–ZnO electrode measured by Brunauer–Emmett–Teller method (Micromeritics Tristar 3000) from N_2 adsorption–desorption isotherms is about 20.9 m^2/g. Pure graphene was also synthesized by direct microwave-assisted reduction of GO solution for comparison.

Under acidic condition of pH <6.0, Zn element exists as Zn^{2+} and $ZnOH^+$ soluble ions in the aqueous solution [41,42]. With the increase of pH value (~9), a conversion from Zn^{2+} and $ZnOH^+$ ions to $Zn(OH)_2$ precipitation happens and finally $Zn(OH)_2$ is transformed to ZnO particles by microwave heating.

$$Zn(OH)_2 \xrightarrow{\text{heating}} ZnO + H_2O \quad (1)$$

The surface morphology, structure and composition of the samples were characterized by high-resolution transmission electron microscopy (HRTEM, JEM-2100), field-emission scanning electron microscopy (FESEM, Hitachi S-4800), atomic force microscopy (AFM, SPI 3800N), X-ray diffraction spectroscopy (XRD, D8 ADVANCE), and energy dispersive X-ray spectroscopy (EDS, JEM-2100), respectively. The UV–vis absorption spectra were recorded using a Hitachi U-3900 UV–vis spectrophotometer. The cyclic voltammetry (CV) and chronopotentiometry experiments were investigated by using Autolab PGSTAT 302N electrochemical workstation in a three-electrode mode, including a standard calomel electrode as reference electrode and a platinum foil as counter electrode. 1 M KCl solution was used as electrolyte. The specific capacitance (C_{sp} in F/g) could be obtained from the CV process according to Eq. (2) or from the charge-discharge process according to Eq. (3):

$$C_{sp} = \frac{\bar{i}}{v \times m} \quad (2)$$

where $\bar{i}$ is the average current (A), v is the scan rate (V/s) and m is the mass of electrode (g).

$$C_{sp} = \frac{i \times t}{\Delta V \times m} \quad (3)$$

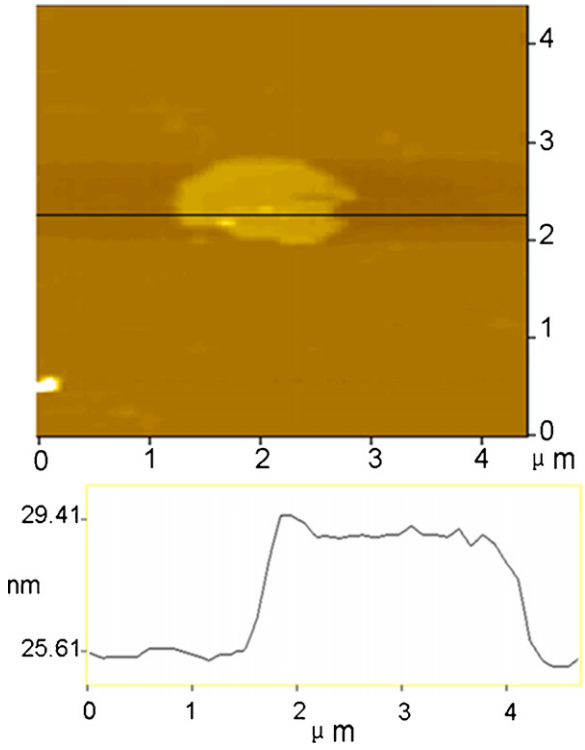

Fig. 1. AFM image of graphene nanosheet.

where i, t and ΔV are the constant current (A), charge/discharge time (s), potential difference (V), respectively.

3. Results and discussion

To indicate the acquirement of graphene, an aqueous solution of graphene was dropped onto the hydrophilic-treated silicon for AFM measurements. Fig. 1 shows the AFM image of as-prepared graphene nanosheet. The height profile of graphene sheet displays a thickness of 3.8 nm, corresponding to the graphene of four or five layers based on theoretical values of 0.78 nm for single layer graphene and the thickness contribution from oxygen-containing groups on the faces [38,43].

Fig. 2(a) and (b) shows the typical FESEM and HRTEM images of as-prepared graphene nanosheets, respectively. The corrugated and scrolled sheets resemble crumpled silk veil waves. Graphene layers interact with each other to form an open pore system, through which electrolyte ions easily access the surface of graphene to form electric double layers [6]. Fig. 2(c) illustrates the FESEM image of graphene–ZnO nanocomposite. It is clearly observed that the surface of curled graphene sheets are packed by nanosized and irregularly shaped ZnO grains, which displays a good combination between graphene sheet and ZnO naoparticles (NPs). Some ZnO NPs are grown on the brink of interlayer and inside interlayer of graphene to form sandwich-like graphene–ZnO structure due to the reduction of Zn^{2+} diffused into the interlayer of GO [41]. Fig. 2(d) and (e) draw the low-magnification and high-magnification HRTEM images of graphene–ZnO nanocomposite. It is clearly seen that the graphene sheets are decorated densely by small ZnO NPs. The diameter of ZnO NPs is estimated to be 5–10 nm and their crystalline structures can be observed clearly from the lattice fringes of the ZnO (0 0 2) plane with an interplanar spacing of approximately 0.52 nm and (1 0 0) plane with an interplanar distance of about 0.28 nm [44,45]. Additionally, the existence of Zn in the nanocomposite has been proved by the peaks of Zn in EDS data (Fig. 2(f)). The appearance of S element and Cu element is due to the residue of reactants

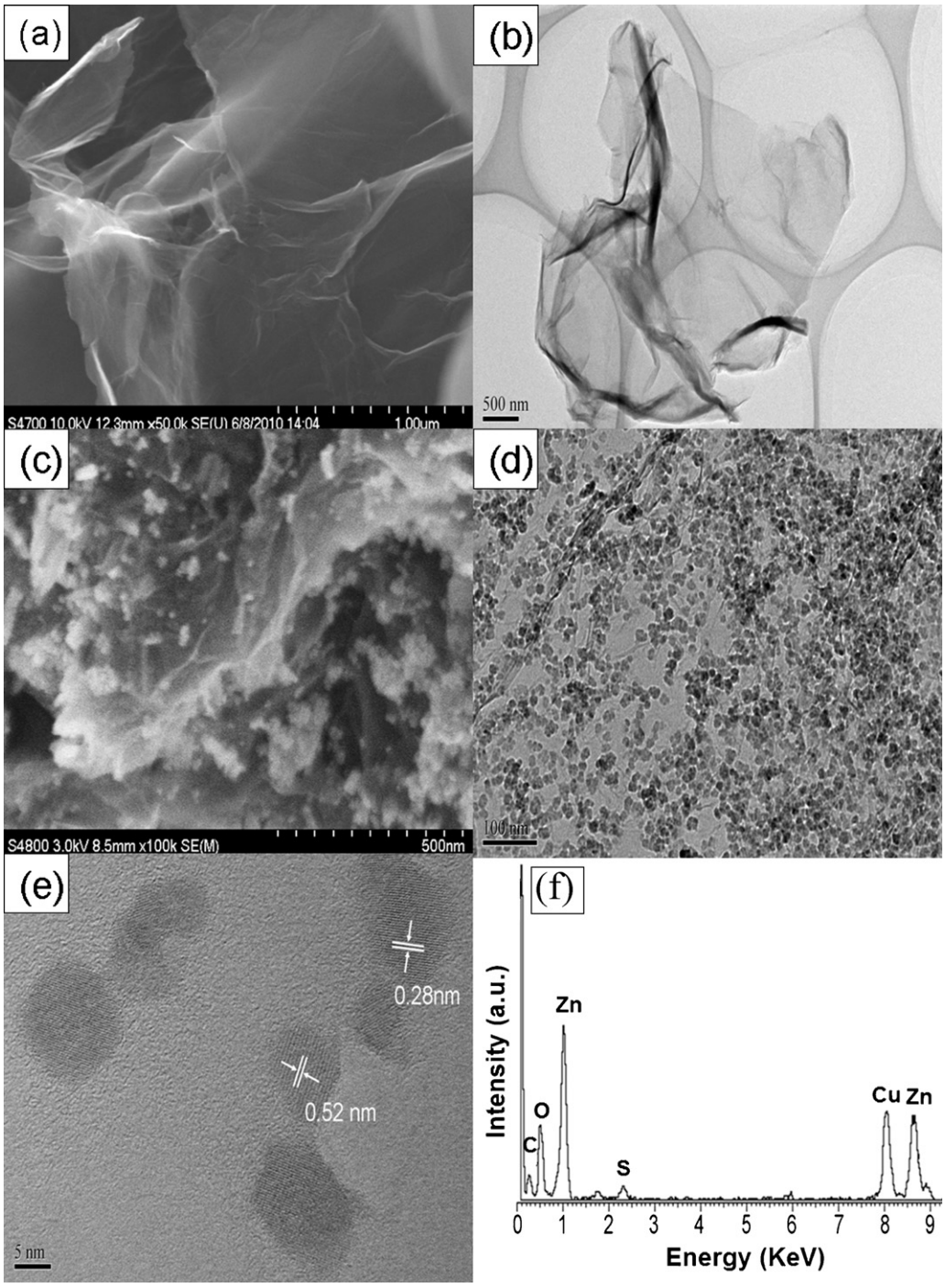

Fig. 2. (a) FESEM and (b) HRTEM images of graphene nanosheets; (c) FESEM, (d) low magnification HRTEM and (e) high-magnification HRTEM images of graphene–ZnO nanocomposite; (f) EDS spectra of graphene–ZnO nanocomposite.

during the synthesis and the use of copper grid for dispersion of sample in EDS test, respectively.

Fig. 3 displays XRD patterns of graphene–ZnO nanocomposite, pure ZnO and pure graphene. Graphene nanosheets exhibit a weak (1 0 0) diffraction peak at 44.5° [46]. The XRD analysis further shows the excellent crystal structures of ZnO NPs even if they are combined with graphene. The peaks at 31.6°, 34.4°, 36.1°, 47.3°, 56.3°, 62.6° and 67.6° correspond to (1 0 0), (0 0 2), (1 0 1), (1 0 2), (1 1 0), (1 0 3) and (1 1 2) planes of ZnO, indicating wutrzite crystal structure [PDF #89-1397].

Fig. 4 shows the UV–vis absorption spectra of graphene and graphene–ZnO nanocomposite. It is observed that graphene exhibits a strong absorption peak at 265 nm which is regarded as the excitation of π-plasmon of graphitic structure [35,47]. Compared with the absorption spectrum of graphene, graphene–ZnO displays a new peak at 362 nm, which is ascribed to the contribution from ZnO NPs. The blue shift in the absorption peak as compared to the one of bulk ZnO is caused by the quantum size-effect of fine structure of nanometer size [48].

CV curves were conducted at a scan rate of 2, 10, 30, 50, 70 and 100 mV/s under the potential from −0.5 to 0.5 V. Fig. 5(a) shows CV curves at a scan rate of 100 mV/s. The shapes of CV loop in our experiment are close to rectangle, indicating a good capacitive behavior in the ESCs [5]. It can be seen that the capacitive per-

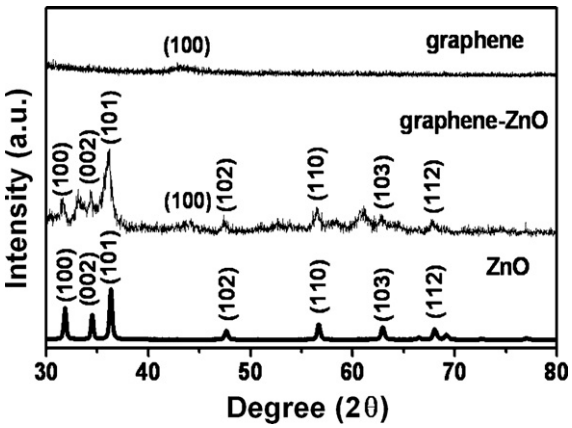

Fig. 3. XRD patterns of graphene–ZnO nanocomposite, pure ZnO and pure graphene.

formance of graphene–ZnO electrode is obviously better than that of pure graphene. Here the capacitive contribution from graphite substrate to the whole electrode is very low and can be neglected [37]. The specific capacitances of graphene–ZnO and graphene calculated from CV curves measured at a scan rate of 2 mV/s are 146 and 59 F/g, respectively. It means that the ZnO contributes to the total capacitance apart from the double-layer capacitance from graphene. Fig. 5(b) shows the plot of scan rate verse specific capacitance of graphene–ZnO nanocomposite. The specific capacitance tends to be relatively stable with the increase in scan rate, accounting for its good discharge efficiency and electrodynamic property.

The charge–discharge behavior of graphene–ZnO electrode was measured by chronopotentiometry from 0 to 1 V at a constant current of 10 mA, as shown in the inset of Fig. 6. The IR drop, caused by the internal resistance of the electrode, is hardly observed owing to the well-formed electrode/electrolyte interface. The stability and reversibility of an electrode material is also critical in the practical application for ESCs [49]. Fig. 6 shows the cyclic performance of the electrode examined by galvanostatic charge–discharge test for 100 cycles. It is observed that the capacitance of graphene–ZnO electrode calculated from charge–discharge curve exhibits little decay during the test, which implies its excellent long-term recycling capability.

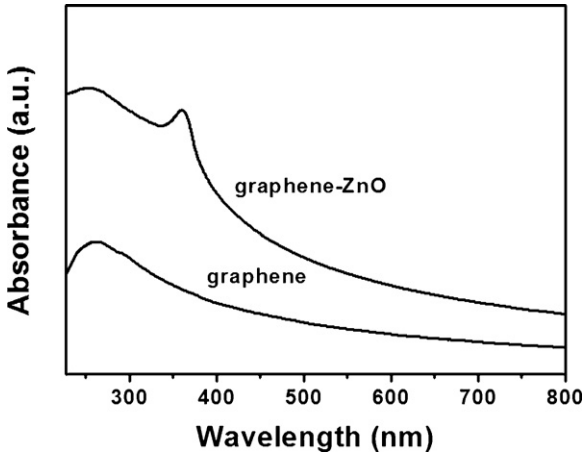

Fig. 4. UV–vis absorption spectra of graphene and graphene–ZnO nanocomposite.

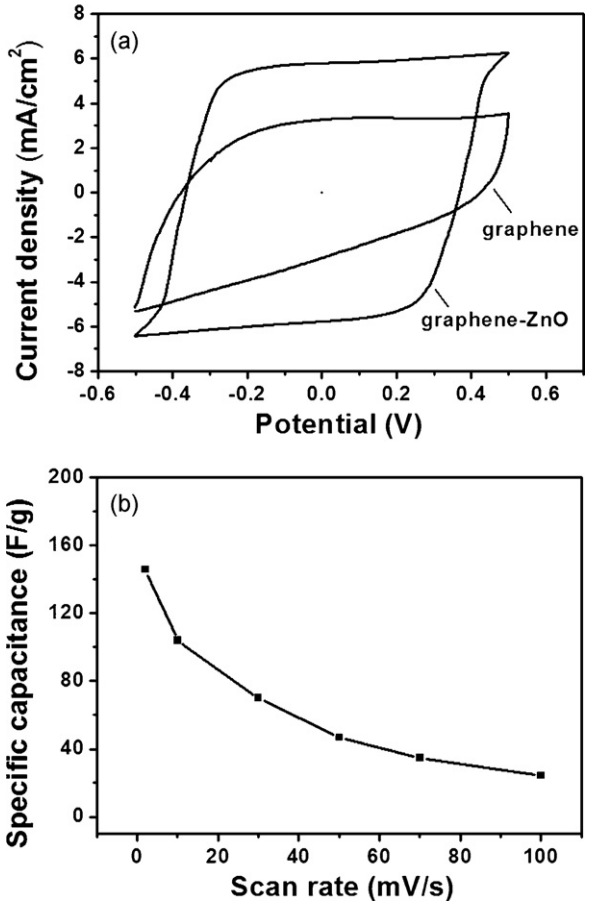

Fig. 5. (a) CV curves of graphene and graphene–ZnO nanocomposite at a scan rate of 100 mV/s; (b) plots of scan rate verse specific capacitance of graphene–ZnO nanocomposite.

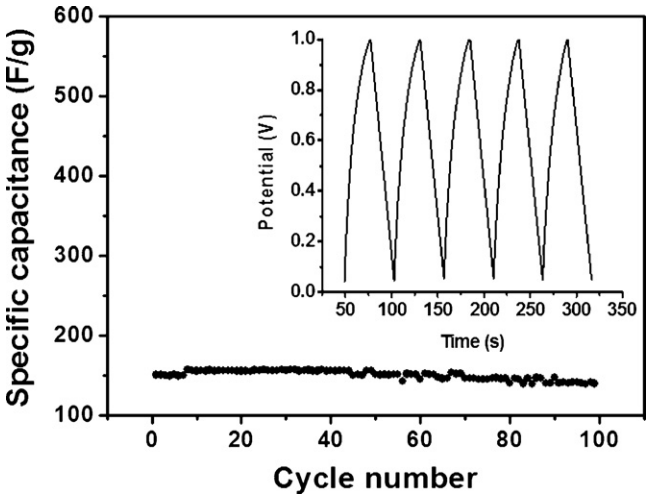

Fig. 6. Cyclic performance of graphene–ZnO nanocomposite. Inset is corresponding charge–discharge curve.

4. Conclusions

Graphene–ZnO nanocomposite was successfully synthesized via microwave-assisted reduction of zinc ions in aqueous solution with GO dispersion. The results of electrochemical experiments indicated that as compared to pure graphene, graphene–ZnO nanocomposite exhibits a better capacitive performance with

joint contribution of capacitance from ZnO and graphene. Graphene–ZnO composite achieves a high capacitance value of 146 F/g and good reversible charge/discharge ability.

Acknowledgements

This work was supported by Special Project for Nanotechnology of Shanghai (no. 1052nm02700) and the Scientific Research Foundation for the Returned Overseas Chinese Scholars.

References

[1] K.S. Novoselov, A.K. Geim, S.V. Morozov, D. Jiang, Y. Zhang, S.V. Dubonos, I.V. Grigorieva, A.A. Firsov, Science 306 (2004) 666.
[2] M.D. Stoller, S. Park, Y. Zhu, J. An, R.S. Ruoff, Nano Lett. 8 (2008) 3498.
[3] X.P. Shen, J.L. Wu, S. Bai, H. Zhu, J. Alloys Compd. 506 (2010) 136.
[4] S.R.C. Vivekchand, C.S. Rout, K.S. Subrahmanyam, A. Govindaraj, C.N.R. Rao, J. Chem. Sci. 120 (2008) 9.
[5] Y. Wang, Z.Q. Shi, Y. Huang, Y.F. Ma, C.Y. Wang, M.M. Chen, Y.S. Chen, J. Phys. Chem. C 113 (2009) 13103.
[6] W. Lv, D.M. Tang, Y.B. He, C.H. You, Z.Q. Shi, X.C. Chen, C.M. Chen, P.X. Hou, C. Liu, Q.H. Yang, ACS Nano 3 (2009) 3730.
[7] J. Yan, T. Wei, B. Shao, F.Q. Ma, Z.J. Fan, M.L. Zhang, C. Zheng, Y.C. Shang, W.Z. Qian, F. Wei, Carbon 48 (2010) 1731.
[8] Q. Wu, Y.X. Xu, Z.Y. Yao, A.R. Liu, C.Q. Shi, ACS Nano 4 (2010) 1963.
[9] Y. Chen, X. Zhang, P. Yu, Y. Ma, J. Power Sources 195 (2010) 3031.
[10] V.C. Tung, M.J. Allen, Y. Yang, R.B. Kaner, Nat. Nanotechnol. 4 (2009) 25.
[11] S. Stankovich, D.A. Dikin, R.D. Piner, K.A. Kohlhass, A. Kleinhammes, Y. Jia, Y. Wu, S. Nguyen, R.S. Ruoff, Carbon 45 (2007) 1558.
[12] Y. Si, E.T. Samulski, Nano Lett. 8 (2008) 1679.
[13] G. Williams, B. Seger, P.V. Kamat, ACS Nano 2 (2008) 1487.
[14] X.L. Li, X.R. Wang, L. Zhang, S.W. Lee, H.J. Dai, Science 319 (2008) 1229.
[15] T.V. Cuong, V.H. Pham, Q.T. Tran, J.S. Chung, E.W. Shin, J.S. Kim, E.J. Kim, Mater. Lett. 64 (2010) 765.
[16] A. Kajbafvala, S. Zanganeh, E. Kajbafvala, H.R. Zargar, M.R. Bayati, S.K. Sadrnezhaad, J. Alloys Compd. 497 (2010) 325.
[17] H.M. Yang, C.H. Huang, X.H. Su, A.D. Tang, J. Alloys Compd. 402 (2005) 274.
[18] T. Thongtem, S. Jattukul, A. Phuruangrat, S. Thongtem, J. Alloys Compd. 491 (2010) 654.
[19] A. Vadivel Murugan, T. Muraliganth, A. Manthiram, Chem. Mater. 21 (2009) 5004.
[20] F.Y. Jiang, Ch.M. Wang, Y. Fu, R.C. Liu, J. Alloys Compd. 503 (2010) L31.
[21] C.T. Lee, F.S. Chen, C.H. Lu, J. Alloys Compd. 490 (2010) 407.
[22] M. Zawadzki, J. Alloys Compd. 451 (2008) 297.
[23] R. Chen, D.H. Chen, J. Alloys Compd. 476 (2009) 671.
[24] Q. Yao, Y.J. Zhu, L.D. Chen, Z.L. Sun, X.H. Chen, J. Alloys Compd. 481 (2009) 91.
[25] W. Chen, L. Yan, P.R. Bangal, Carbon 48 (2010) 1146.
[26] Z. Li, Y. Yao, Z. Lin, K.S. Moon, W. Lin, C. Wong, J. Mater. Chem. 20 (2010) 4781.
[27] I. Janowska, K. Chizari, O. Ersen, S. Zafeiratos, D. Soubane, V.D. Costa, V. Speisser, C. Boeglin, M. Houlle, D. Begin, D. Plee, M.J. Ledoux, C. Pham-Huu, Nano Res. 3 (2010) 126.
[28] Y.J. Kim, J.H. Lee, G.C. Yi, Appl. Phys. Lett. 95 (2009) 213101.
[29] X.Y. Zhang, H.P. Li, X.L. Cui, Y. Lin, J. Mater. Chem. 20 (2010) 2801.
[30] J. Yao, X.P. Shen, B. Wang, H.K. Liu, G.X. Wang, Electrochem. Commun. 11 (2009) 1849.
[31] J. Shen, Y. Hu, M. Shi, N. Li, H. Ma, M. Ye, J. Phys. Chem. C 114 (2010) 1498.
[32] S.M. Paek, E.J. Yoo, I. Honma, Nano Lett. 9 (2009) 72.
[33] T.N. Lambert, C.A. Chavez, B. Hernandez-Sanchez, P. Lu, N.S. Bell, A. Ambrosini, T. Friedman, T.J. Boyle, D.R. Wheeler, D.L. Huber, J. Phys. Chem. C 113 (2009) 19812.
[34] S.R. Kim, M.K. Parvez, M. Chhowalla, Chem. Phys. Lett. 483 (2009) 124.
[35] J. Wu, X. Shen, L. Jiang, K. Wang, K. Chen, Appl. Surf. Sci. 256 (2010) 2826.
[36] F. Li, J. Song, H. Yang, S. Gan, Q. Zhang, D. Han, A. Ivaska, L. Niu, Nanotechnology 20 (2009) 455602.
[37] T. Lu, Y.P. Zhang, H.B. Li, L.K. Pan, Y.L. Li, Z. Sun, Electrochim. Acta 55 (2010) 4170.
[38] H.B. Li, T. Lu, L.K. Pan, Y.P. Zhang, Z. Sun, J. Mater. Chem. 19 (2009) 6773.
[39] Y.X. Xu, H. Bai, G.W. Lu, C. Li, G.Q. Shi, J. Am. Chem. Soc. 130 (2008) 5856.
[40] H.A. Becerril, J. Mao, Z. Liu, R.M. Stoltenberg, Z. Bao, Y. Chen, ACS Nano 2 (2008) 463.
[41] X. Chen, Y. He, Q. Zhang, L. Li, D. Hu, T. Yin, J. Mater. Sci. 45 (2010) 953.
[42] K. Tetsuo, I. Hiroaki, J. Cryst. Growth 283 (2005) 490.
[43] X.B. Fan, W.C. Peng, Y. Li, X.Y. Li, S.L. Wang, G.L. Zhang, F.B. Zhang, Adv. Mater. 20 (2008) 4490.
[44] S.K. Park, J.H. Park, K.Y. Ko, S. Yoon, K.S. Chu, W. Kim, Y.R. Do, Cryst. Growth Des. 9 (2009) 3615.
[45] L.Q. Jiang, L. Gao, Mater. Chem. Phys. 91 (2005) 313.
[46] L. Tang, Y. Wang, Y. Li, H. Feng, J. Lu, J. Li, Adv. Funct. Mater. 19 (2009) 2782.
[47] X. Wang, L.J. Zhi, N. Tsao, J.L. Tomovic, K. Mullen, Angew. Chem. Int. Ed. 47 (2008) 2990.
[48] X.M. Yang, Z.Z. Gu, Z.H. Lu, Y. Wei, Appl. Phys. A 59 (1994) 115.
[49] Z.A. Hu, Y.L. Xie, Y.X. Wang, L.P. Mo, Y.Y. Yang, Z.Y. Zhang, Mater. Chem. Phys. 114 (2009) 990.